

## **Chemical controls on ferrierite crystallization during diagenesis of silicic pyroclastic rocks near Lovelock, Nevada**

**STEPHEN B. RICE\***

Exxon Research and Engineering Company, Annandale, New Jersey 08801, U.S.A.

**KEITH G. PAPKE**

2180 Schroeder Way, Sparks, Nevada 89431, U.S.A.

**DAVID E. W. VAUGHAN**

Exxon Research and Engineering Company, Annandale, New Jersey 08801, U.S.A.

### **ABSTRACT**

The zeolites ferrierite, mordenite, and clinoptilolite have formed with smectite through hydration reactions in a sequence of rhyolitic pyroclastic rocks near Lovelock, Nevada. High activities of silica and magnesia were required simultaneously for the large-scale crystallization of ferrierite in these diagenetically altered rocks. Post-depositional addition of Mg coincided with ferrierite and smectite formation. The source of the Mg is not known, but it could have originated either from a brackish, saline lake or from nearby leached basalts. Thus, origins of the Lovelock ferrierite deposit may have involved both lacustrine deposition and an open ground water system for the transformation of vitric tuffs into zeolites.

Ferrierite crystallized early, mainly in the pore space of the tuffs. Clinoptilolite and cristobalite grew later by replacement of glass shards. Orthoclase and mordenite crystallized somewhat later, orthoclase usually in intimate association with ferrierite in K-rich zones and mordenite alone in open pore spaces. Ferrierite crystallization proceeded through a mechanism of dissolution and reprecipitation on glass and clay surfaces. Significant variation in chemical composition of individual ferrierite crystals occurs on the scale of a few cubic millimeters.

### **INTRODUCTION**

Ferrierite is a medium-pore zeolite that has interesting potential applications in petrochemical processing. Knowledge of the conditions leading to its formation may provide insight into creating a simple, inexpensive synthesis method. The Lovelock, Nevada, deposit, in which ferrierite occurs in minable proportions, provides a natural laboratory for studying the processes of zeolitization and the conditions under which ferrierite crystallizes. What were the special conditions responsible for the unusually large quantity of ferrierite at Lovelock? From the results of a study of ferrierite synthesis, Cormier and Sand (1976) concluded that metastability may be the key. Their conclusion, although soundly based on experiment and intuitively pleasing when applied to the Lovelock deposit, nevertheless requires further examination through careful study of the mineralogical and chemical relationships in the rocks themselves. In this study we have combined electron petrographic characterization with bulk chemical and phase assemblage data to interpret the origins of ferrierite in altered pyroclastic rocks.

Since its discovery in an outcrop of olivine basalt near the shore of Kamloops Lake in British Columbia (Graham, 1918), the zeolite ferrierite has been observed in nearly 30 localities. With the exception of a very few occurrences in altered volcanogenic sediments, these all appear to be hydrothermal vug occurrences. In the deposit near Lovelock, discovered in 1965 by P. E. Galli, ferrierite formed through hydration reactions in a sequence of rhyolitic pyroclastic rocks. A puzzle at Lovelock is the dominance of ferrierite over mordenite and clinoptilolite, two zeolites that are very common in similar tuffaceous settings in the western United States. In fact, several zeolites, including erionite, mordenite, chabazite, clinoptilolite, and analcime, are very common in such deposits, whereas ferrierite is only known to occur in the Lovelock deposit and in smaller amounts in the Stillwater Range near Fallon, Nevada. A Korean occurrence was interpreted by Noh and Kim (1986) to result from diagenesis of silicic vitric tuffs.

Reports describing the Lovelock zeolite deposit contain widely divergent opinions about the genesis of the zeolites. Sand and Regis (1968) suggested a hydrothermal origin for the ferrierite, but no supporting evidence for estimates of temperature or source of the fluids was given. Regis (1970) described the Lovelock and Stillwater Range

\* Present address: Exxon Production Research Company, P.O. Box 2189, Houston, Texas 77252-2189, U.S.A.

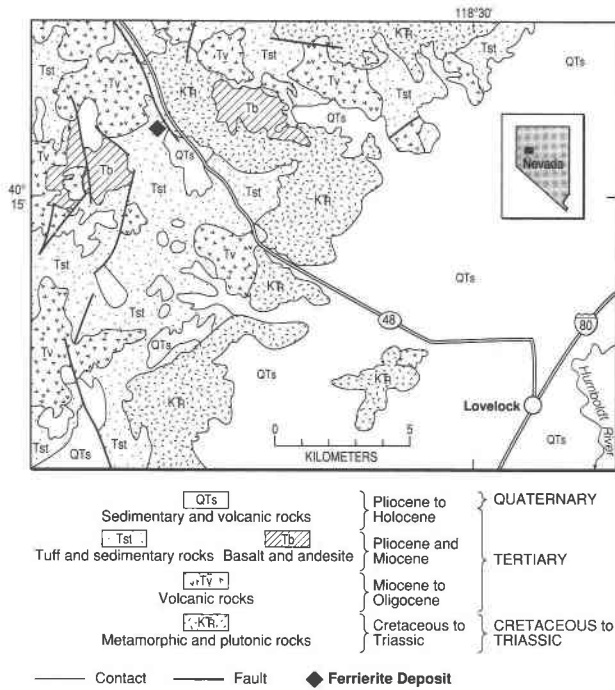


Fig. 1. Location map for the Lovelock zeolite deposit (Sheppard et al., 1983).

occurrences of central Nevada, giving compositions of the ferrierite at each locality, and he also reported zonation for ferrierite, mordenite, and clinoptilolite based on outcrop sampling. Low alkalinity conditions were suggested. In a guidebook accompanying the zeolite fieldtrip Zeo-Trip '83, Sheppard et al. (1983) described the Lovelock occurrence in somewhat greater detail and concluded that the original pyroclastic material was deposited in a lake but that little was known about the fluids responsible for zeolitization. An examination of the chemical controls on zeolite crystallization in the Lovelock deposit that account for this unusual occurrence is the subject of the present study.

**BACKGROUND**

**Geologic setting of the Lovelock deposit**

The Lovelock zeolite deposit occurs in a group of unnamed sedimentary and volcanic rocks of Tertiary age (Miocene or Pliocene) in a small valley within the Trinity Range (T. 28 N., R. 30 E.) in Pershing County, northwest Nevada (Fig. 1). Reconnaissance mapping placed the Lovelock deposit in the Upper Tertiary volcanic group (Tuv) of Stewart and Carlson (1978). The ferrierite deposit of the Stillwater Range also lies within the Upper group. The observable surface features of the deposit and the core locations are shown in Figure 2.

The stratigraphy based on the bulk chemistry, petrography, and phase-assemblage data is shown in Figure 3. There is a zonation characterized by mordenite at the top, grading downward into less mordenite and increasing amounts of ferrierite, and finally a large amount of glassy

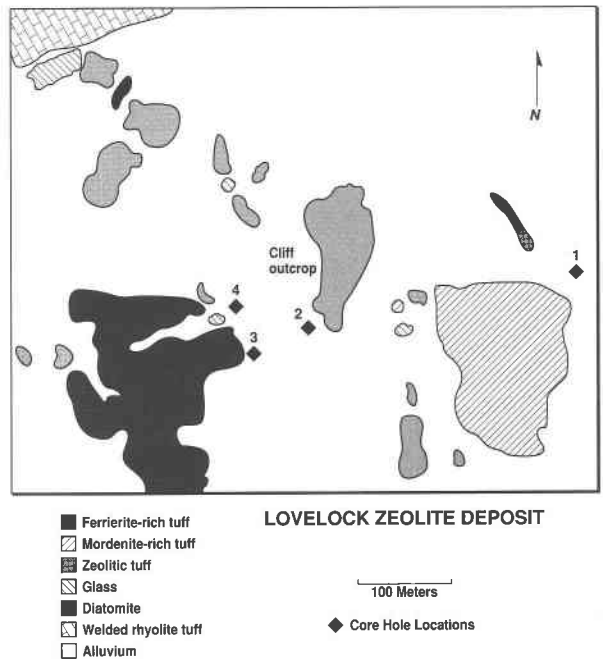


Fig. 2. Geologic map of the Lovelock deposit.

material. This sequence agrees with the order of appearance of these zeolites deduced from the experiments of Cormier and Sand (1976). The cores themselves, however, are more difficult to correlate. The discontinuities between cores 2, 3, and 4 could be fault-bounded discontinuities or unconformities related to variations in the sedimentary environment such as erosional surfaces or pinch-outs.

**Cores and outcrop samples**

Four vertical core holes (Fig. 2), each 5 cm (2 in.) in diameter, were drilled under contract for W. R. Grace and Company in the early 1970s. Portions of the cores

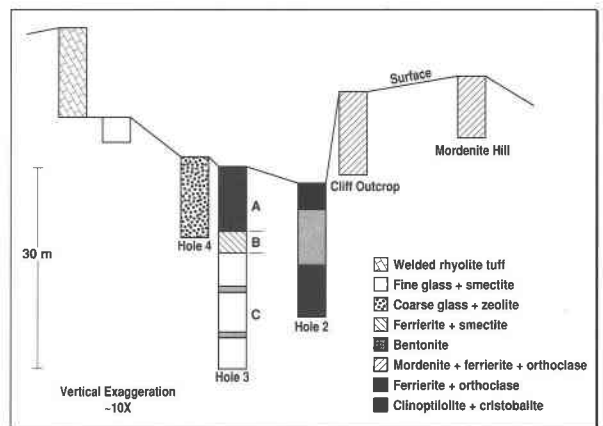


Fig. 3. Stratigraphy of the Lovelock zeolite deposit. Layers A, B, and C are defined on the basis of composition (as in Fig. 14) and assemblage.

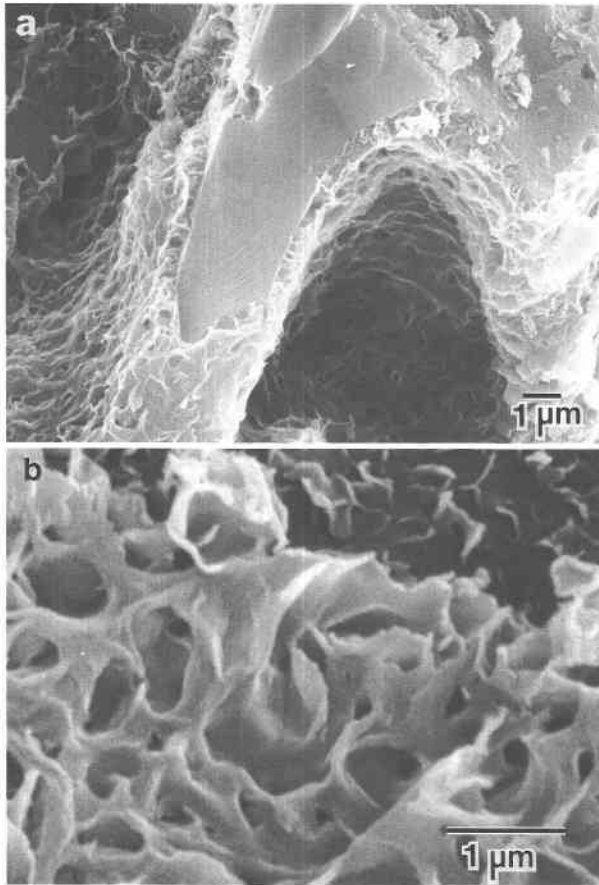


Fig. 4. SEM micrograph showing (a) a fracture section of glass in sample SR75 and (b) the morphology of smectite on the glass surface.

are stored at the Nevada Bureau of Mines and Geology in Reno, Nevada. Samples were selected from the four cores, with particular attention paid to the best preserved cores from hole nos. 2 and 3. Unfortunately, the lower core from hole no. 3, below about 12.2 m, was inadvertently discarded at W. R. Grace and Company.

Vitric and zeolitic tuffs were sampled in outcrop to augment the core samples. The ferrierite-rich outcrops were surprisingly difficult to sample because of their extreme toughness. They have a green color that is subtly different from the other outcrops of tuffs, most of which are buff to tan. They are also locally strongly silicified, although the spatial relationship between the opaline zones and the ferrierite tuff was not clear in the available outcrops. There is banding in many of the zeolitic tuffs, and some sedimentary features, such as ripple marks, pinch-outs, and cross-bedding relationships, were preserved despite the zeolitization process.

#### Instrumental techniques

Powder X-ray diffraction (PXRD) was carried out using powder-pack methods with an automated Siemens D500

diffractometer with  $\text{CuK}\alpha$  radiation. Scans were run at  $2^\circ$  per min from  $2$  to  $60^\circ 2\theta$ , at 40 kV and 30 mA. Phase identification, particularly for zeolites, was enhanced by a computer-based matching program with a library of natural and synthetic zeolites as well as other silicates.

The scanning electron microscope used was a JEOL 35C equipped with an  $\text{LaB}_6$  gun, a four-crystal wavelength spectrometer (WDX), adjunct energy-dispersive X-ray detector (EDX), and PGT System IV analysis system. Both normal secondary electron imaging (SEI) and backscattered electron imaging (BEI) were used. Electron microprobe analysis was performed by a method combining EDX and WDX, using orthoclase from Benson Mines, St. Lawrence County, New York (K, Al, Si), labradorite plagioclase from Lake County, Oregon (Ca, Al, Si), and hornblende from Kakanui, New Zealand (Mg, Ti, Fe, Al), as standards. Alkali diffusion during analysis of zeolites and glass was corrected by monitoring counts for 30 s and extrapolating to zero time. Clay and zeolite analyses totaled less than 100% primarily because of the presence of  $\text{H}_2\text{O}$ , both adsorbed and structural. Ferrierite typically has 10–15%  $\text{H}_2\text{O}$  by weight. Matrix corrections were calculated by the NBS Frame C program. The secondary ion mass spectrometer (SIMS) used was a Cameca 3f with a high-gain camera (20 million ASA) and a Crystal image processor (Leta, 1985). Because the charging problems inherent with the imaging SIMS method are more severe than with SEM, SIMS samples required embedding in a conductive mount.

A Philips 420ST transmission electron microscope (TEM) with EDX and adjunct PGT System IV analysis system was used for characterization of glassy and zeolitic tuffs and for identification of zeolites by electron diffraction. Chemical compositions of ferrierite crystals were determined using the Cliff-Lorimer thin-film method (Goldstein et al., 1977).

## RESULTS

### Electron petrography

**Vitric tuffs.** Vitric tuff from 30.5-m depth in hole no. 3 is relatively unaltered. Glass constitutes most of the specimen, and the remainder is quartz, plagioclase, and phenocryst sanidine and Fe-Ti oxides. These are clearly air-fall tuffs because, in addition to good sorting (average shard size is 50–100  $\mu\text{m}$ ), there is a large amount of interclast porosity and no evidence for either welding or flow.

A fine-grained unaltered ash (SR73) outcrops at the base of the welded tuff at the northern edge of the field area. These are angular shards exhibiting elongated pores and occasional cusped morphology and whose average grain size (5–10  $\mu\text{m}$ ) is very similar to the Hekla  $\text{H}_4$  tephra layer. Heiken and Wohletz (1985) interpreted those to be of phreatoplinian origin, implying a highly vesicular magma resulting from mixing with surface  $\text{H}_2\text{O}$ .

Figure 4 shows fresh, fractured glass shards (50–100  $\mu\text{m}$  grain size) from SR75 and SR76 with smectite rims, which have this feature in common with C3-30.5. Smec-

tite, the predominant authigenic phase in the early stages of alteration, is present on most of the glass surfaces observed. The morphology shown in Figure 4b is typically observed for smectite, although at least in some instances, this corn-flake texture may be an artifact of the preparation for SEM.

SIMS images from polished sections of specimen C3-30.5 in Figure 5 illustrate several salient features of these slightly altered shards. The K ion image indicates that alkalis have not been leached from this glass, a conclusion also inferred from the composition of the glass (Table 1) because Na (3.02% Na<sub>2</sub>O) and K concentrations (5.25% K<sub>2</sub>O) are typical of rhyolites with about 78% SiO<sub>2</sub>. The Mg image and corroborating TEM examination clearly show that Mg is concentrated in the smectite phase rimming the glass. Therefore, the glass alteration here appears to be limited to the surface of the shards.

Cristobalite, clinoptilolite, and possibly amorphous silica are pseudomorphic after shards (Fig. 6) and thus form in replacement reactions in several hole 2 tuffs. Ferrierite is present in only minor amounts and occurs as coatings on shards. Figure 7a shows in cross section a relict pumice shard that is now largely cristobalite. Much of the silica reported in this study is probably the opal-CT phase defined by Jones and Segnit (1971), characterized by lepispheres composed of intersecting platelets of disordered  $\alpha$  cristobalite. Because the 4.3-Å tridymite peak characteristic of opal-CT was not always observed, we refer to it throughout as cristobalite. The pores, which appear nearly circular in this view, are a composite of authigenic orthoclase and ferrierite, lined with smectite. The orthoclase crystals, distinguishable in powder X-ray patterns from sanidine phenocrysts, form an elliptical pattern that suggests a concentration gradient of K with ellipsoidal symmetry. Figure 7b shows a void outlined by smectite and ferrierite in succession. It is not known whether there is any direct relationship between the zeolite and the clay in terms of nucleation, crystallographic control, chemical exchange, or reaction. Probably the clay merely provided a substrate on which the ferrierite could grow because ferrierite was also observed to have grown directly on remnant glass surfaces in specimens C2-3.7 and C4-8.5.

Products occur at shard edges and in pores in the hole-2 and hole-4 tuffs, which have carried the alteration process further than the early smectite alteration stage represented by specimen C3-30.5. These additional crystals attached to shards (Fig. 8a) have a morphology and composition confirming their identity as ferrierite. They appear physically separated from glass by a clay layer. Ferrierite typically develops in a prismatic habit normal to the shard surfaces (Fig. 8b). There are very large, highly vesicular pumiceous grains and blocky, nonvesicular shards. Perlitic texture is very common in some of the blocky nonporous particles.

Some bentonitic beds are interspersed with glassy and zeolitic tuffs. In certain strata the smectite is pure enough to be considered for recovery, along with the zeolite, were the deposit to be mined commercially.

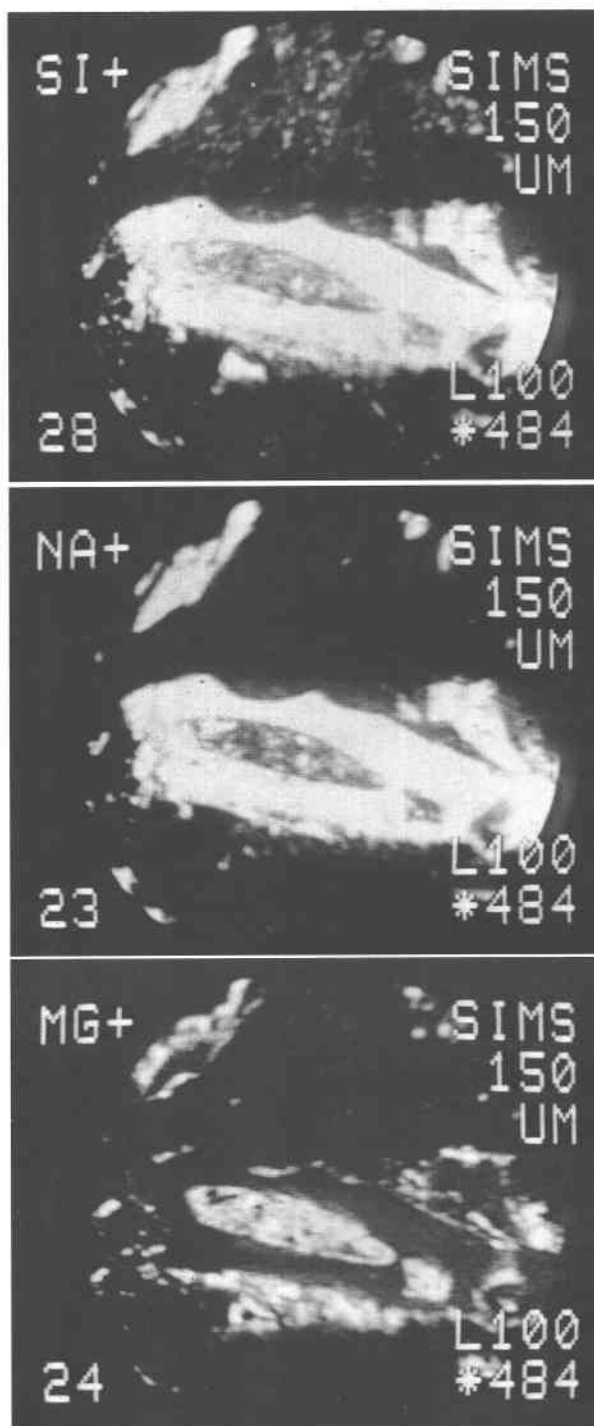


Fig. 5. SIMS images of a polished section of vitric tuff sample C3-30.5. The Si image identifies the shape of the glass shard. The Na image, which imitates Si here, confirms that alkalis are uniformly present in the glass and therefore leaching has not occurred. The Mg is a constituent of the smectite coating the glass.

TABLE 1. Glass compositions

	1	2	3	4	5	6	7	8
SiO <sub>2</sub>	75.0	74.2	73.5	74.4	77.1	74.8	76.2	75.7
Al <sub>2</sub> O <sub>3</sub>	11.8	11.9	11.8	12.2	12.9	12.2	12.4	12.4
MgO	0.00	0.00	0.00	0.00	0.00	0.00	0.05	0.14
CaO	0.22	0.17	0.28	0.22	0.00	0.31	0.00	0.89
Na <sub>2</sub> O	2.88	2.83	2.71	3.27	4.60	4.59	5.33	4.12
K <sub>2</sub> O	5.13	4.86	5.04	5.10	5.76	4.40	4.49	4.26
TiO <sub>2</sub>	0.00	0.00	0.00	0.00	0.00	0.00	0.00	0.00
FeO	0.00	0.00	0.00	0.00	0.00	0.00	0.00	0.00
Total	95.02	94.00	93.40	95.12	100.35	96.25	98.48	97.51
Remarks					vesicular	vesicular	nonvesic.	nonvesic.
Sample no.	C3-30.5	C3-30.5	C3-30.5	C3-30.5	SR78	SR78	SR78	SR78

**Ferrierite tuffs.** These tuffs have been converted to assemblages of ferrierite, authigenic orthoclase, cristobalite, and minor mordenite. Some of these tuffs are nearly pure ferrierite. The chemical compositions of several ferrierite samples from Lovelock are given in Table 2. Like other ferrierite samples (Wise and Tschernich, 1976), these are magnesian. The tuffaceous ferrierite samples from the Lovelock, Stillwater, and South Korean occurrences, however, have distinctively high K concentrations.

There are several manifestations of the preservation of the microscopic vitroclastic texture. One of these takes the form of ferrierite and authigenic potassium feldspar in a dense, fine-grained intergrowth (Fig. 9) in which the orthoclase inhabits the periphery of former shards. Another feature is the presence throughout the tuffs of shard-shaped voids. It is not always obvious whether particular voids represent primary porosity or secondary porosity introduced by the dissolution of glass. Those voids with definite cusped pumice morphologies appear to be dissolved shards. That early ferrierite crystals grew into primary pores is supported by the observation in core 4 tuffs of ferrierite crystal growth on fairly fresh glass shards. Where ferrierite was permitted to crystallize in an unconstrained space the morphologies represented in Figure 10 were observed. A third feature is the occurrence of cristobalite, which is commonly found as spherical polycrystals, often seen along or adjacent to remnant vitric outlines. In Figure 6 the cristobalite spheres are just visible within the limbs of the relict shards. The K SIMS image in Figure 11, which clearly distinguishes the orthoclase

from the ferrierite, also shows the vitroclastic texture. Phenocryst sanidine contains significant concentrations of Na, whereas the authigenic orthoclase contains almost none (Table 3). This allows the two feldspars to be easily differentiated by SIMS or EDX analysis when the grain size or textures are not definitive.

**Mordenite tuffs.** Although most zeolitic tuffs contain both ferrierite and mordenite, the predominance of mordenite in some tuffs made textural distinctions possible. Close inspection of Figures 12a and 12b reveals a fine, lacelike network of authigenic orthoclase and cristobalite, apparently positioned at former rims of glass shards. This microtexture was also observed in the ferrierite tuffs, but the contrast between zeolite-filled void space and the narrow network of orthoclase and cristobalite was not so well developed as in the mordenite-rich tuffs. Note also the presence in Figure 12b of a double-walled network mainly composed of orthoclase. The space between the walls appears to be void. The mordenite tuffs are in general much more porous than ferrierite-rich tuffs because the mordenite grows, with few exceptions, as bundles and radial sheaves of prismatic crystals. These (e.g., Fig. 12a) are morphologically indistinguishable from acicular ferrierite. In contrast to the intimate intergrowth of ferrierite with orthoclase, in which the individual crystallites are often not discernible by SEM, no similar textures were observed for mordenite.

Typical Lovelock mordenite and clinoptilolite compositions are given in Table 4. The somewhat unusual composition for the clinoptilolite (high Si/Al and high

TABLE 2. Ferrierite chemical analyses

	1	2	3	4	5	6	7	8	9	10
SiO <sub>2</sub>	69.7	69.9	69.3	72.9	70.4	70.1	76.2	73.5	73.7	69.6
Al <sub>2</sub> O <sub>3</sub>	10.6	10.3	10.9	11.4	10.0	12.1	11.6	11.3	11.3	11.1
MgO	0.48	1.98	2.51	3.13	1.61	1.95	1.74	1.89	2.19	2.48
CaO	1.74	0.99	1.46	1.06	0.61	0.74	2.78	2.89	2.10	1.72
Na <sub>2</sub> O	1.18	0.30	0.20	0.59	0.01	0.01	0.00	0.08	0.30	0.30
K <sub>2</sub> O	4.11	4.12	4.01	3.64	5.05	5.46	1.70	1.97	2.56	2.96
TiO <sub>2</sub>	0.40	0.01	0.27	0.45	0.04	0.00	0.70	0.68	0.48	0.21
FeO	0.82	0.25	0.73	1.36	0.23	0.45	1.41	1.45	1.21	0.66
Total	89.02	87.90	89.45	94.55	87.89	90.80	96.14	93.71	93.83	89.01
Remarks	matrix	matrix	matrix	vug	matrix	matrix				
Sample no.	KP52	KP52	KP52	KP52	SR64	SR64	C2-14.3	C2-14.3	C2-17.4	C2-17.4

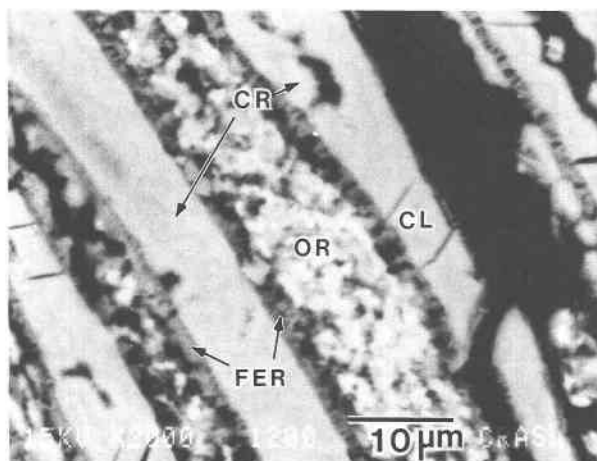


Fig. 6. Backscattered electron image of a cross section of sample C2-3.7 showing replacement of glass by clinoptilolite (CL) and cristobalite (CR). Ferrierite (FER) and orthoclase (OR) formed between the limbs of the shard. Some of the ferrierite has grown normal to the former glass surface. Note also that cristobalite spheroids occur as discrete crystallites within the limbs.

Ca) makes a note concerning heulandite group nomenclature worthwhile. The zeolites heulandite and clinoptilolite have the same framework structure and are distinguished on the basis of composition [heulandite if  $Ca > (Na + K)$  according to Mason and Sand, 1960, or if  $Si/Al < 4$  according to Boles, 1972] or structural stability upon heating to 450 °C (heulandite if the structure collapses, according to Mumpton, 1960). Our phase (Table 4, analyses 3 and 4) could be termed heulandite on the basis of cations because  $Ca > (Na + K)$  or clinoptilolite on the basis of framework  $Si/Al$  ratio ( $\sim 4.8$ ). We did not perform the heating test. We call this phase clinoptilolite because heulandite rarely has a sedimentary occurrence, whereas clinoptilolite and mordenite have a frequent association in altered tuffs (e.g., Gottardi and Galli, 1985), particularly in high-silica environments.

#### Paragenetic sequence

One of the first changes attending glass alteration at Lovelock was the crystallization of smectite rich in Mg, Ca, and Fe as an abundant shard-rimming phase (e.g., in specimens C3-100 and SR74-76). The appearance of clay, and in particular smectite, is a frequently observed phenomenon in altered glasses of a range of compositions. Smectite was reported, for instance, by Broxton et al. (1987) in altered rhyolitic glasses at Yucca Mountain, Nevada; by Keller et al. (1971) in altered rhyolite near a hot spring in Michoacan, Mexico; and by Boles and Coombs (1975) as the first phase of alteration in Triassic tuffs of andesitic through rhyolitic composition. Davies et al. (1979) reported smectite-coated glass grains in the first alteration zone of Guatemalan andesitic volcanoclastics. Sheppard and Gude (1968) reported smectite as a remnant phase adjacent to altered glassy shards in the tuffs

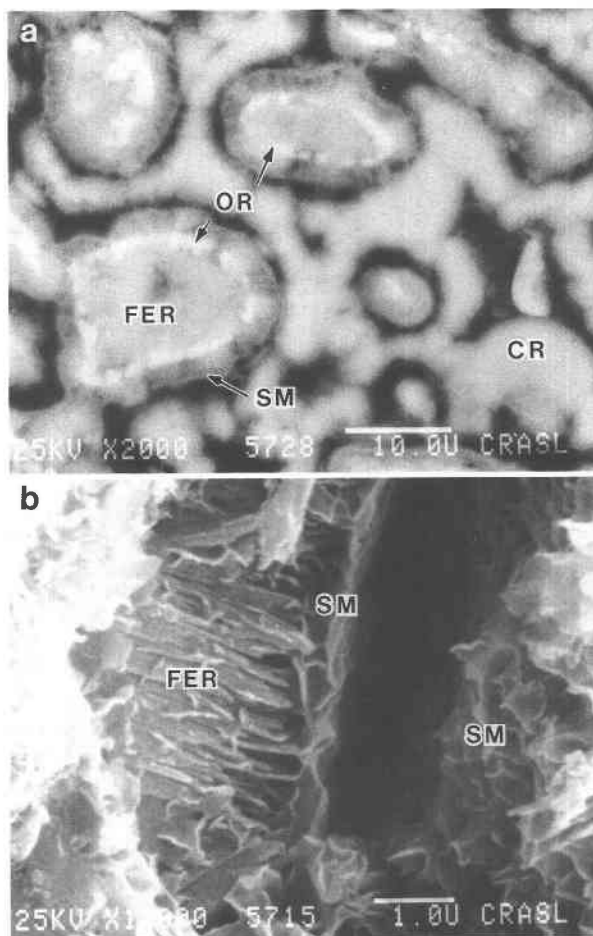


Fig. 7. (a) Back-scattered electron image of sample C2-17.4 showing orthoclase (OR), ferrierite (FER), and smectite (SM) filling the pores of a relict shard. The shard walls are the connected curvilinear features separating rounded pores. Some of this wall material is now cristobalite (CR). (b) Fracture section of sample C2-17.4 showing empty pore space (black) rimmed by smectite and ferrierite.

of Lake Tecopa, a saline, alkaline lake. Other examples include Boles and Surdam (1979), Brey and Schmincke (1980), and Hay (1963). Smectite may not always precede zeolitization, but it clearly is an early stage of hydration

TABLE 3. Feldspar chemical analyses

	1	2	3	4
SiO <sub>2</sub>	68.7	69.1	72.1	69.3
Al <sub>2</sub> O <sub>3</sub>	15.3	18.7	14.8	18.0
MgO	0.28	0.80	0.68	0.00
CaO	0.81	0.32	0.58	0.44
Na <sub>2</sub> O	0.25	0.00	0.23	3.10
K <sub>2</sub> O	13.2	11.1	11.2	8.67
TiO <sub>2</sub>	0.00	0.00	0.00	0.01
FeO	0.00	0.00	0.00	0.65
Total	98.41	100.00	99.62	100.18
Type	orthoclase	orthoclase	orthoclase	sanidine
Sample no.	KP52	C2-14.3	C2-17.4	SR3

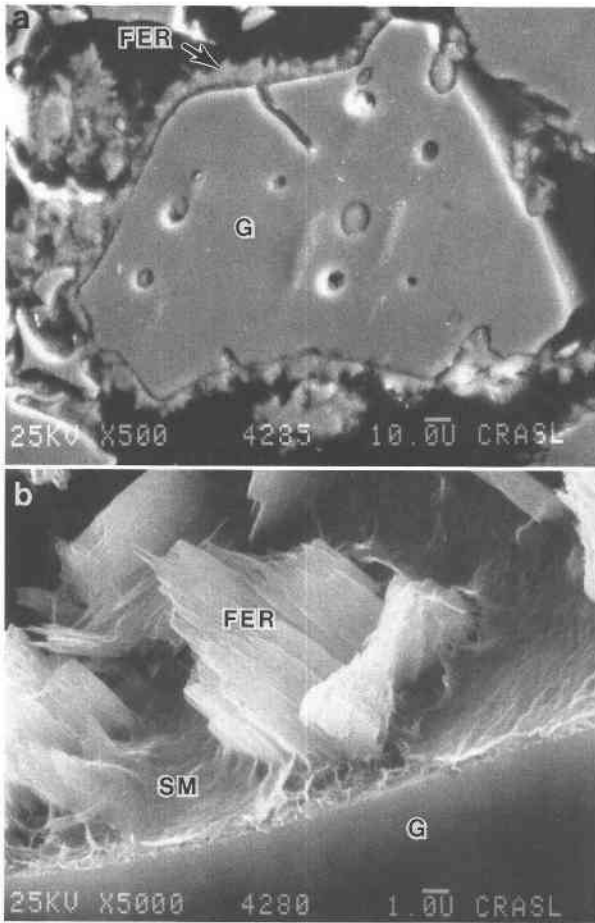


Fig. 8. (a) Cross section of a single glass shard (G) with ferrierite at its periphery. (b) Higher magnification image of ferrierite (FER) and smectite (SM) adjacent to the glass. Microanalysis and morphology confirmed the identify of ferrierite.

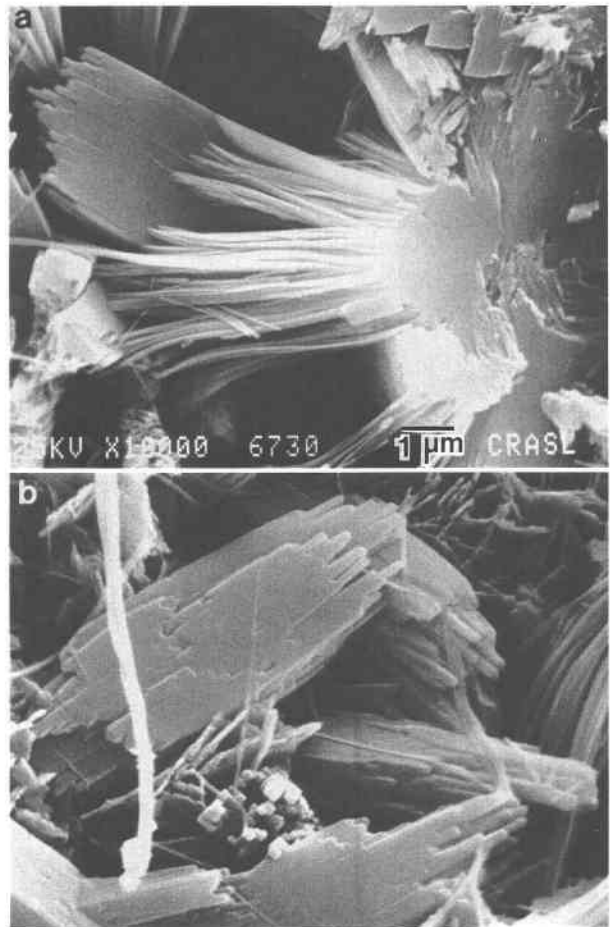


Fig. 10. Fracture section of sample SR67 showing ferrierite habits. (a) Radiating bundle of fibers. (b) Boxy acicular crystals.

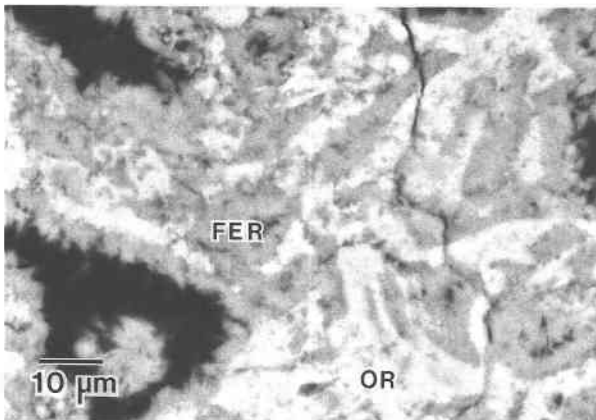


Fig. 9. Backscattered electron image of cross section of densely intergrown ferrierite and orthoclase (ferrierite tuff SR67), the latter showing the relict shard position.

alteration of the unstable natural glasses. Hay (1963) showed that the early-formed clay in the John Day Formation, resulting from percolating ground waters, was an important agent in altering the water chemistry, rendering it favorable for zeolite crystallization by raising the pH.

There are several reasons for suggesting that ferrierite is probably the first zeolite to appear in the transformation of glass: (1) ferrierite occurs on silica and clay substrates in core 2 tuffs, in combination with orthoclase and smaller amounts of clinoptilolite, (2) ferrierite coexists with glass and clay in core 4 tuffs, and (3) the vertical zonation within the deposit as a whole shows a progression from glass to ferrierite to mordenite.

At Lovelock, cristobalite and clinoptilolite cocrystallized as replacements for dissolving glass, probably after the onset of the crystallization of ferrierite, mordenite, and orthoclase. The occasional draping of mordenite on clinoptilolite (SR1.5) suggests that, at least in those particular tuffs, mordenite postdated the clinoptilolite.

Based on their coexistence in many tuffs, mordenite growth occurred during or after ferrierite crystallization.

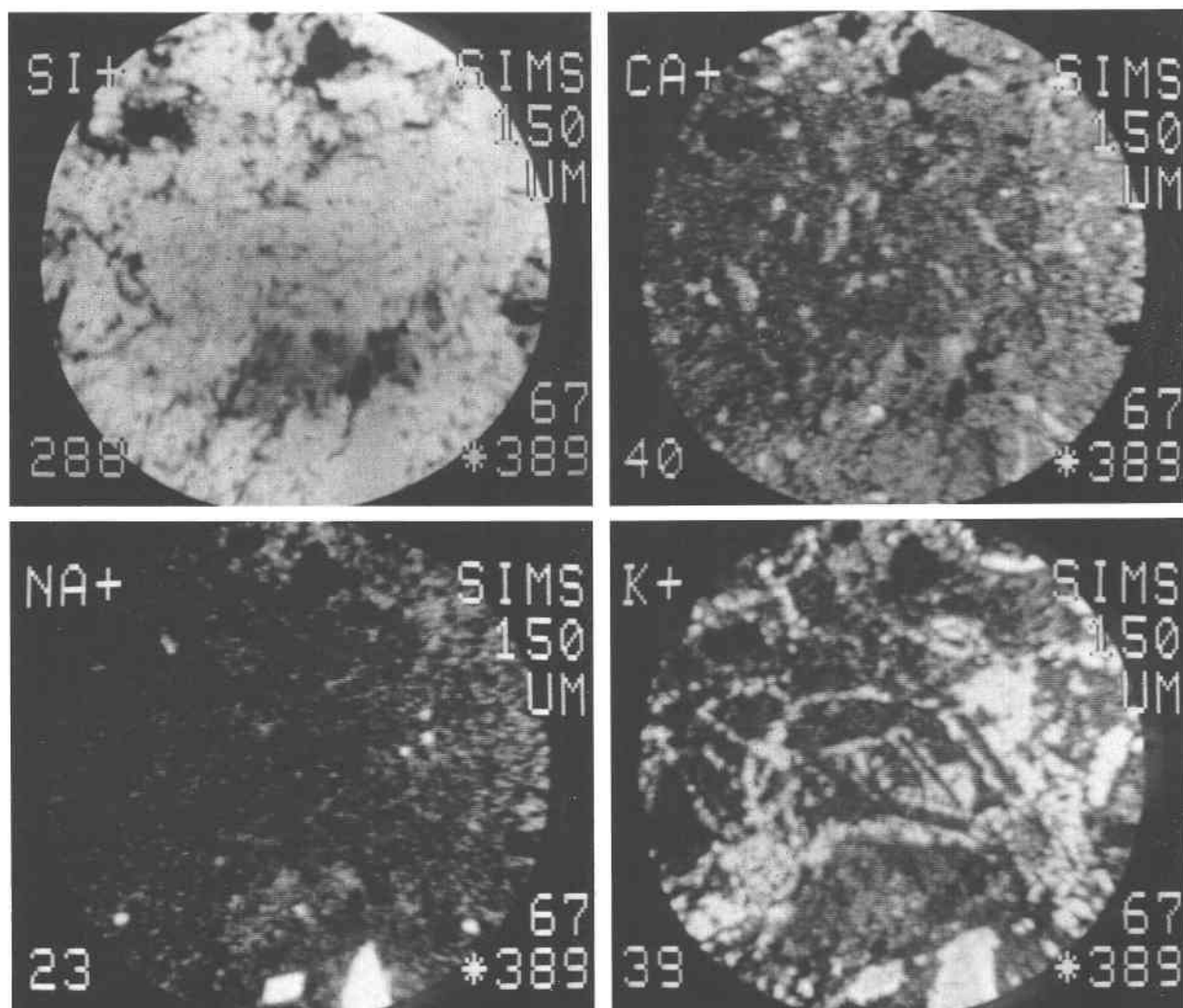


Fig. 11. SIMS images of a cross section of sample SR67. Most of the areas of high K concentration represent orthoclase. The two grains in the bottom of the field are sanidine pyroclastic grains.

There is no convincing evidence that one crystallized at the expense of the other. Both ferrierite and mordenite crystallize into open pore space in the tuffs, but there was no evidence from TEM characterization that these two zeolites crystallized in close proximity in the fashion that ferrierite and orthoclase did. The textural preference of mordenite for filling pores produced by elimination of shard grains, requiring as it does an advanced stage of glass dissolution, is interpreted to occur later than the intimate growth of ferrierite and orthoclase.

Cristobalite is a minor to major phase in the hole no. 2 tuffs as well as in some ferrierite tuffs. It also coexists with clinoptilolite and orthoclase, but there was no petrographic evidence of the time relationship of cristobalite and ferrierite.

Orthoclase appears to have been the last phase to crystallize. The orthoclase textures in the ferrierite tuffs, such as its presence at the periphery of former shards or con-

centric to adjacent shard pore outlines, could indicate crystallization contemporaneous with ferrierite. In these instances, orthoclase crystallization occurred along zones of microchemical enrichment of K and Al. Overgrowths and crack-fillings of orthoclase-rich material suggest that in those instances it persisted after the main episode of zeolitization.

Figure 13 schematically summarizes the paragenetic sequence of authigenic phases in the Lovelock deposit.

#### BULK CHEMICAL AND MINERALOGICAL TRENDS

##### Bulk chemistry of core hole no. 3

Bulk chemical data for core samples from hole no. 3 (Fig. 14) suggest that several distinct units are represented in the 30-m thick deposit of rhyolite pyroclastics. Although the average pyroclast grain size, as inferred from the textures in SEM images, seems to be relatively con-

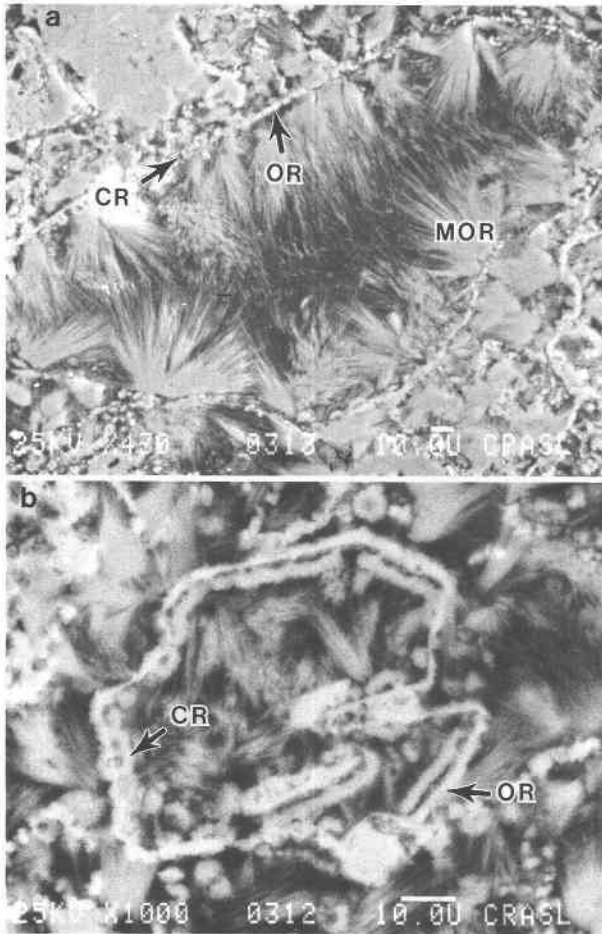


Fig. 12. Cross sections of mordenite tuff SR3 showing (a) individual void space, outlined by orthoclase crystallite network and partially filled with prismatic mordenite, (b) double-walled texture of orthoclase and minor cristobalite.

stant over the entire length of core 3, the chemical variations require the recognition of several distinct units. Phase identification based on PXD helped in delineating the zones. From the surface to about 10 m is a ferrierite-rich zeolitic zone (layer A), containing some authigenic orthoclase and cristobalite but whose mineral content approaches pure ferrierite in some places. These tuffs appear to have the same mineralogical characteristics as the ferrierite-rich rocks that crop out in the southwest corner of the area. Between 10 and 12.5 m is an Mg-rich, low Si/Al zone (layer B) containing ferrierite and smectite. At about the 12.5-m level there is a break in the dominant assemblage. Below 12.5 m ferrierite is absent and, with the exception of some clay-rich beds and pyroclastic fragments, only vitric ash (layer C) is present. Judging from the material recovered at 30 m, smectite rims probably occur on most of the glass shards below 12.5 m, even in those beds that are primarily vitric. This indicates that, although smectite alteration preceded ferrierite formation, not all of the clay-altered tuffs were zeolitized. The

TABLE 4. Mordenite (1, 2) and clinoptilolite (3, 4) chemical analyses

	1	2	3	4
SiO <sub>2</sub>	66.6	68.3	72.8	76.8
Al <sub>2</sub> O <sub>3</sub>	10.2	10.8	13.2	13.5
MgO	0.00	0.00	1.16	0.84
CaO	2.05	2.17	4.00	4.71
Na <sub>2</sub> O	0.24	0.97	0.45	0.20
K <sub>2</sub> O	0.84	1.10	0.96	0.78
TiO <sub>2</sub>	0.01	0.00	0.00	0.00
FeO	0.09	0.08	0.00	0.00
Total	80.02	83.32	92.59	96.87
Remarks	vug filling	vug filling	rhombus	rhombus

composition of this clay is Mg rich, as distinct from later clays, which were determined by TEM/EDX to be Fe rich. These later clays occur as thin alteration products on ferrierite laths and are not considered important in the context of ferrierite genesis. As shown in Table 5, layers A and B both have higher MgO than does layer C. Because the initial bulk chemical compositions of A, B, and C were probably comparable, zeolite-forming reactions must have involved some additional chemical transformation specific to the tuffs shallower than 12.5 m.

Bulk compositions of the upper zeolitic tuffs in hole no. 3 show decreasing alkali-metal concentrations with depth (Fig. 14). In the near-surface tuffs of layer A the K<sub>2</sub>O concentration (6–8%) is higher than in fresh rhyolite, but K<sub>2</sub>O gradually decreases to a relatively low value in layer B. Na content also decreases downward over this interval, whereas Ca increases gradually. The SEM data support the presence of K-enriched zones within the layer A tuffs, and it may be that there is more authigenic feldspar in the near-surface tuffs. Many examples of K<sub>2</sub>O enrichment, such as authigenic orthoclase overgrowths on relict pyroclastic feldspars and feldspar-rich veinlets in the zeolitic tuffs, reflect the presence of a K-rich fluid. The question remains whether the K and Na were added from an external source or reflect variations in original tuff chemistry. Fractionation of K<sub>2</sub>O is not uncommon in some ignimbrite flow sequences, such as the Bishop Tuff (Hildreth, 1979) and the Valley of Ten Thousand Smokes (Mahood, 1986), in which increasingly less silicic lavas extrude onto earlier more silicic flows. However, if this were the case, K<sub>2</sub>O and Si/Al values from the base of layer B to the top of layer A in hole no. 3 would be expected to decrease. They demonstrate precisely the opposite trend. It also seems unlikely that concentrations varying by a factor of 4 over just 15 m would result from continuous changes in the source chemistry or that an air-fall pyroclastic deposit would reliably record these changes. A more probable explanation is the addition of alkali-rich fluids or K-rich fluids that partially exchanged with Na in the deposit, thus reducing the total Na concentrations below typical values for rhyolites.

#### Mass balance

In order to understand the chemistry of zeolitization, particularly with respect to ferrierite crystallization, it is

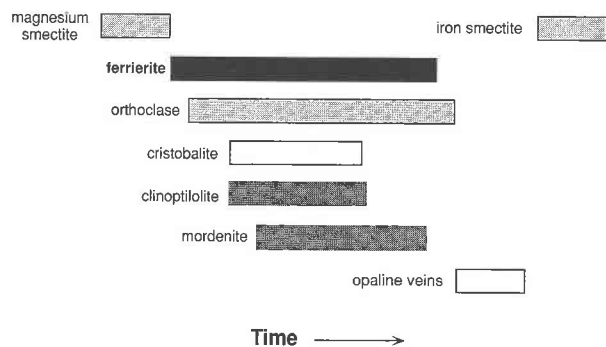


Fig. 13. Paragenetic sequence of authigenic minerals recognized in the Lovelock deposit.

necessary to determine whether the reactions were isochemical or required significant fluxes of material. Changes in elemental concentrations were calculated assuming that the composition of core 3 vitric tuffs of layer C was representative of the original tuffs from which the zeolites formed. Layers A and B were considered individually. It is not known a priori that any of the components were truly immobile or insoluble during the hydration reactions. The compositions were calculated on an H<sub>2</sub>O-free basis in order to determine the relative change in A and B from C. Rhyolites or obsidians usually contain only a few percent H<sub>2</sub>O, whereas ferrierite tuffs have approximately 10% H<sub>2</sub>O. It was also assumed consistent with metasomatism that the volume of the pyroclastic tuffs remained approximately constant during the process. This is the metasomatic assumption. The following relationship was used to calculate  $\Delta$  values:

$$\Delta_{\text{oxide}} = 100(\text{oxide}_A \cdot \rho_A - \text{oxide}_C \cdot \rho_C / \text{oxide}_C \cdot \rho_C) \quad (1)$$

in which oxide<sub>A</sub> is the weight percent of the oxide in layer A and  $\rho_A$  is the density of tuff layer A. The equivalent equation for layer B relative to layer C was also applied.

There are at least two possibilities that explain the differences between layers A, B, and C: (1) that they were separate and chemically different units to begin with, or (2) that concentration changes were produced by the addition or subtraction of material. Both may be correct. Layers A and B have lower Na contents than does C, which suggests leaching. The fate of the Na is not clear, however. Because the K concentration tends to be relatively high and that of the Na low, an alternative mechanism is coupling through exchange reactions. The observations suggest that the reactions assisting zeolite crystallization were not isochemical. All three layers have much higher Mg, higher Ca, and lower Na concentrations than would be expected for a rhyolite. The large relative differences determined for A and B with respect to C suggest also that these were deposited separately. The Al-, Fe-, and Mg-rich composition of layer B suggests that it originally had a larger mafic component than did layer A.

Because ferrierite is a high-silica zeolite, a high activity of silica in the zeolite-forming fluids is required. Many of

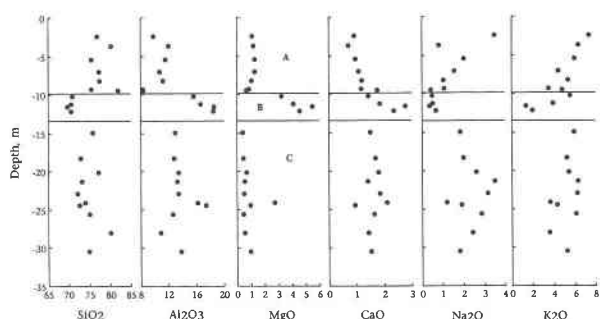


Fig. 14. Variation of element concentrations with depth in hole no. 3 tuffs. Layer A is predominantly ferrierite and orthoclase. Layer B is predominantly ferrierite and smectite. Layer C is glass and clay.

the vug occurrences in andesite and basalt have linings of chalcedony in intimate contact with ferrierite (Gottardi and Galli, 1985). The presence of cristobalite implies the presence of free silica during the zeolite diagenesis in the Lovelock deposit. Abundant opaline rocks visible in outcrop are further evidence.

The total Mg content of the original rhyolite, only about 0.5% MgO, was insufficient to account for the vast quantities of ferrierite in the Lovelock deposit. The addition of Mg in the form of smectite coatings on glass shards appears to be responsible for most of the Mg necessary for ferrierite formation.

#### Ferrierite crystal chemistry

Several populations of ferrierite samples were identified by electron microprobe analysis, namely, a group with Mg/Ca of 2.5 to 3.0 and a group with Mg/Ca of about 0.5. Both compositional groups are represented in KP52 (e.g., Table 2, analyses 1 and 2) and SR64 tuffs. During TEM/EDX work, substantial variation in Si, Mg, and Ca concentrations was observed for crystals from tuff specimens as small as 1 mm<sup>3</sup> (Fig. 15). The grouping of ferrierite compositions into high and low Mg/Ca groups ap-

TABLE 5. Mass balance in hole no. 3 ferrierite tuffs\*

Oxide	Upper (A) ferrierite zone (7)**	Lower (B) ferrierite zone (4)**	Vitric tuff hole 3 (6)**	$\Delta$ (A), %	$\Delta$ (B), %
SiO <sub>2</sub>	77.8	71.46	75.0	-2.0	-10.0
Al <sub>2</sub> O <sub>3</sub>	10.3	16.49	12.73	-23	+22
Na <sub>2</sub> O	1.50	0.78	2.59	-45	-72
K <sub>2</sub> O	5.39	3.74	5.33	-4.5	-34
MgO	1.06	3.57	0.63	+59	+435
CaO	1.12	1.98	1.61	-34	+16
Fe <sub>2</sub> O <sub>3</sub>	1.32	2.75	1.79	-0.30	+45
TiO <sub>2</sub>	0.15	na†	0.15	0	na†
Total	98.64	98.02	99.83		

\* Mass changes for layers A and B assuming C is the original composition (dry basis) using Equation 1 with bulk compositions of core 3 tuffs.

\*\* Number of samples averaged in parentheses.

† The abbreviation na = not analyzed.

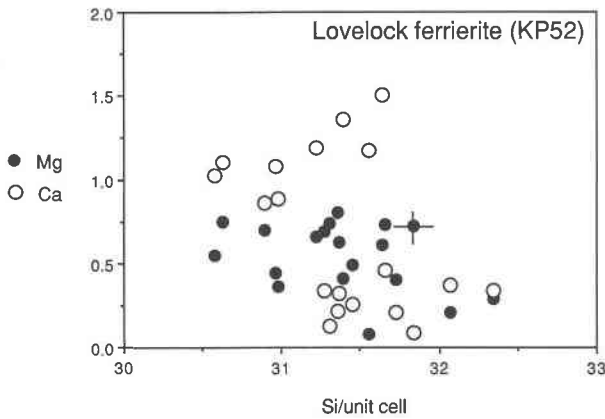


Fig. 15. Divalent cation concentrations vs. Si for individual ferrierite crystals from a small chip of ferrierite tuff (KP52). Data were obtained from TEM/EDX analyses, based on unit-cell contents of 72 O atoms.

pears to be a consequence of Ca concentration differences. Another grouping of ferrierite compositions occurs in the core 2 tuffs but in smaller amounts than in core 3 tuffs. The cluster of three calcic ferrierite compositions in Figure 16, outside the compositional field defined by bulk zeolitic tuff, probably reflects in part a chemistry inherited from the original core 2 tuff.

Compositions of glass, ferrierite, and smectite demonstrate the chemical control of the precursor glass and added smectite on the resultant ferrierite (Fig. 16). The ferrierite compositions (solid circles) reside between the alkali-rich glass and the (Mg + Ca)-rich smectite (open circle). Two inferences can be drawn from this. First, the ferrierite in the Lovelock deposit, although alkali-rich compared with many other ferrierite compositions, has too much Mg to be derived in large quantity from the pristine glass and H<sub>2</sub>O alone. All known natural ferrierite samples have at least 0.5% MgO. Second, the mordenite compositions (solid squares in Fig. 16) and the clinoptilolite compositions (open squares) are too calcic to be derived from the glass + H<sub>2</sub>O + smectite. This is one key to the subordination of mordenite and clinoptilolite relative to ferrierite in this locality because it is not likely that either mordenite or clinoptilolite could accept such large amounts of Mg and remain stable.

To sum up: Mg occurs at significant concentrations in all of the known natural ferrierite occurrences. The Mg concentration per unit cell, based on 72 O atoms, ranges from approximately 0.4 to nearly 3, averaging around 2 (Sameshima, 1986). The Lovelock ferrierite, although it has a small Mg content compared with many others, nevertheless required the addition of substantial Mg to the silicic glass for development in large quantities. Mg has a specific site in the ferrierite structure, for which it is especially suited, and it is not easily removed by acid leaching (Vaughan, 1966). These observations strongly

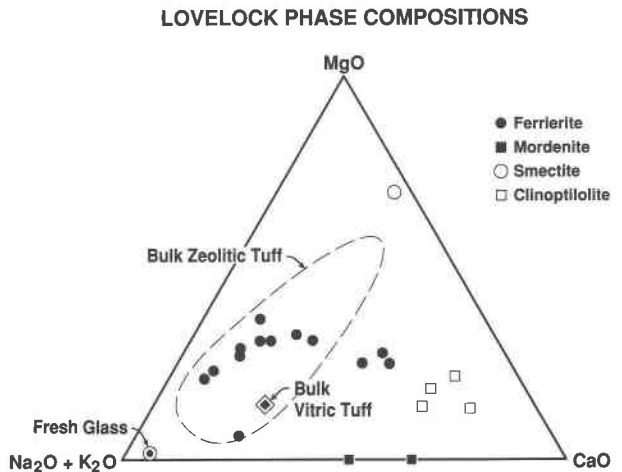


Fig. 16. Normalized MgO-(Na<sub>2</sub>O + K<sub>2</sub>O)-CaO contents (wt%) for Lovelock zeolites and tuffs. The dashed field represents about 40 bulk analyses of tuffs from Lovelock.

indicate a fundamental role of Mg-bearing fluids in the formation of ferrierite in the Lovelock deposit.

## DISCUSSION

### Comparison of Lovelock tuffs with other silicic pyroclastic tuffs

Of the many potential controls on ultimate zeolite assemblages, one that is constrained at Lovelock is the bulk glass starting composition, represented by the fresh glass analyses of C3-30.5, SR78, and C4 tuffs. The chemical compositions representative of the three layers A, B, and C in core 3 are given in Table 5. In Figures 17a-17d, Lovelock compositions are compared with those of approximately 40 other pyroclastic glassy rhyolites from the literature. It was desirable to have the most direct comparison with like tuffs, namely, pyroclastic fall deposits of silicic composition, rather than the whole rhyolitic suite. Some of these have zeolites associated with them, but most do not. Chemical data were obtained for Lovelock glass compositions by electron microprobe analysis, SIMS imaging, and TEM/EDX. Lovelock bulk ash (layer C) has approximately two times more MgO and about one and one-half times more CaO than other pyroclastic rhyolites with the same SiO<sub>2</sub> content (Figs. 17a, 17b). The MgO (<0.05 wt%) and CaO (~0.2 wt%) concentrations determined for the interior of the Lovelock shards were right on the trend for a silica value of 78%.

When the compositions of layers A and B are compared with the silicic trend, it is found that MgO and CaO contents are, in general, much higher than expected for silicic glassy tuff of the same silica content. K concentrations are typical for rhyolites, whereas Na concentrations are about a factor of 2 below normal. Thus, although layer C has apparently not been significantly leached of Na, layers B and C probably have been, sug-

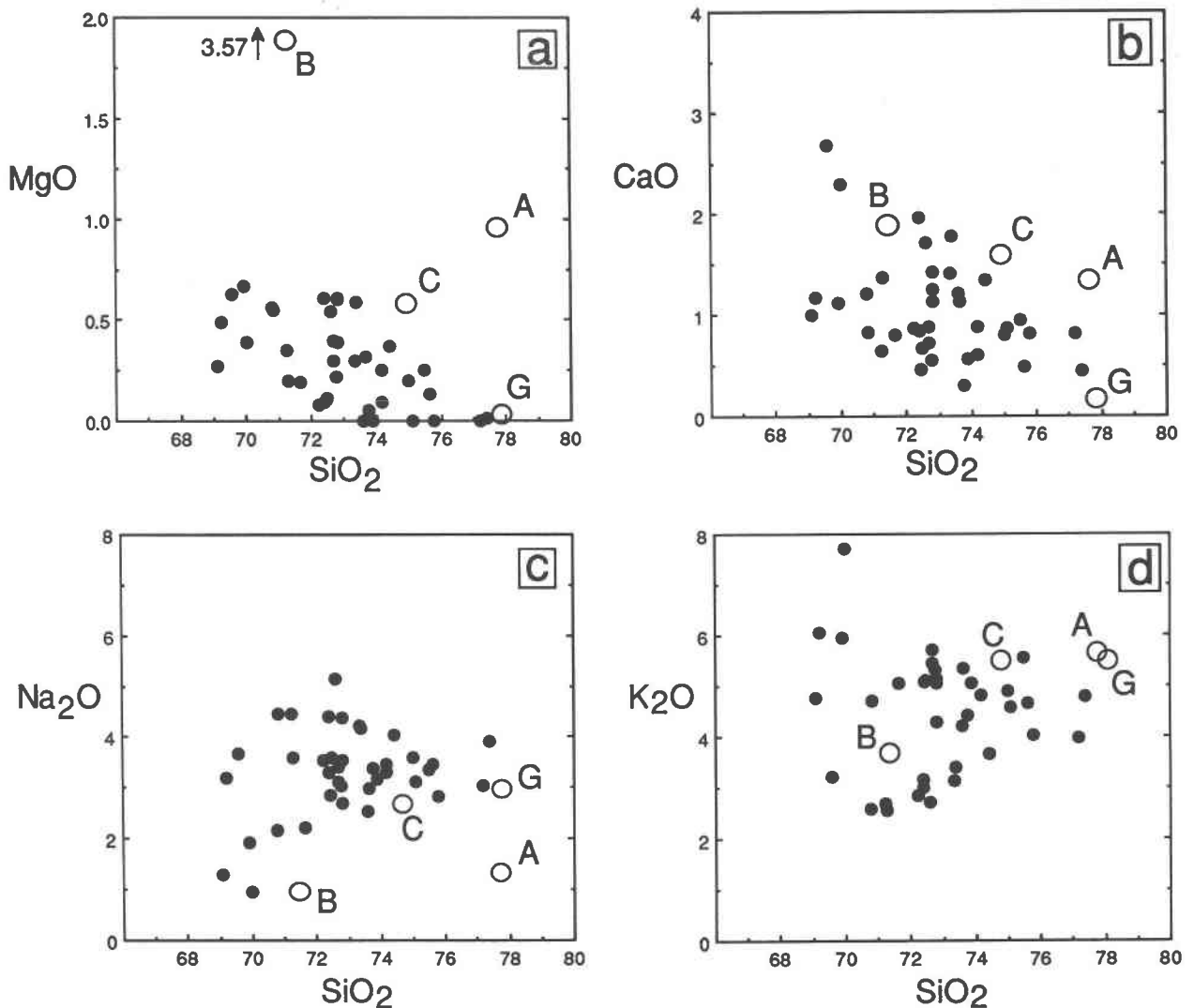


Fig. 17. Diagrams of variations in element concentrations for bulk analyses from silicic pyroclastic tuffs. Data taken from literature sources are solid circles; Lovelock layers A, B, and C, as well as the fresh Lovelock glass (G) in layer C, are represented by large open circles.

gesting that in addition to the clay formation, other hydration reactions accompanied zeolitization.

#### Geological setting

Of the many sources of aqueous fluids in which zeolites occur, those possibly important for the Lovelock deposit are hydrothermal, percolating ground water, and lacustrine. There is an absence of minerals diagnostic of hydrothermal activity. The widespread silicification does have the appearance of a fused material, but this feature need not be a high-temperature reaction because the silica could be derived from feldspar-forming reactions at low temperature. The authigenic feldspar itself, authigenic orthoclase, although perhaps representative of the highest temperature or highest grade of alteration attained at Lovelock, need not be of hydrothermal origin. For these reasons, a hydrothermal origin seems unlikely.

Lacustrine deposition could well be involved, as evidenced by the presence of diatomite beds, authigenic feldspars that commonly occur in saline, alkaline lake deposits (Hay, 1966), and the relatively sharp boundary between the zeolite tuffs and the underlying glassy beds. From SEM observations of morphological characteristics, the diatoms were identified as *Melosira crenulata* or *Melosira granulata*. As far as the authors are aware, these species are not constrained by salinity. If connate lake water is invoked as the sole agent of alteration, the pH of the water could not have exceeded about 9 without dissolving much of the opaline silica. The fairly sharp contact between vitric tuff and ferrierite tuff in hole no. 3 could be interpreted several ways. One interpretation would favor a lacustrine depositional environment because the bottom of the lake would be represented by an abrupt break. A fault juxtaposing relatively fresh tuffs

with highly zeolitized tuffs could also explain the discontinuity. The vertical changes in alkali concentrations and the presence of diatomaceous beds could both be due to the presence of a relatively freshwater lake. However, the results of mass-balance calculations described above, which show addition of both Mg and K and the removal of Na, strongly argue for an open ground water system.

#### Chemical and textural development during diagenesis

Because of the widespread occurrence of Mg-rich clay coatings on the glass shards and the relatively minor concentrations of alkaline-earth cations in the fresh glass, it is inferred that  $Mg^{2+}$  and  $Ca^{2+}$  were added to the vitric pile by aqueous fluids sometime during or after deposition. This could have been accomplished through either the presence of brackish connate  $H_2O$  derived from a saline lake or by leaching of nearby basalts and transport of Mg and Ca to the Lovelock site. The smectite also had important implications for the textural development of the deposit. The Lovelock zeolite tuffs, as do most other zeolite tuffs, preserved a vitroclastic texture inherited from the precursor ash. Textural observations made in this study point to early smectite as a key factor in this process. The presence of smectite at the peripheries of shard grains was responsible for preserving the vitroclastic texture, whereas the porous nature of the coating permitted glass dissolution to proceed. Stanley and Benson (1979) observed hollow clay coatings of smectite cements in vitric rocks from which detrital grains had been dissolved. The observed variations in Mg content of the Lovelock ferrierite samples noted earlier could be caused by the proximity of the crystallizing ferrierite to smectite or by variation in smectite composition.

The widespread occurrence of authigenic orthoclase at Lovelock is a feature that was not fully recognized in previous descriptions of the deposit. According to a study by Sheppard and Gude (1973), zonation of minerals often occurs in lacustrine zeolite deposits where saline minerals are interbedded with zeolites. These typically exhibit a sequence proceeding from glass under freshwater conditions to zeolites under moderately saline conditions to potassium feldspar and scapolite under highly saline conditions. No saline minerals have been recognized in the deposit. Thus, rather than indicating the extent of diagenesis in a highly saline environment, crystallization of orthoclase in the Lovelock deposit may be more a consequence of high K activity in the altering fluids.

Cristobalite and clinoptilolite formed as diagenetic replacements of glass shards. One of the petrographic features observed (e.g., C2-17.3) was relict shards replaced by silica and discrete crystals of clinoptilolite. This replacement was probably the result of a dissolution-precipitation mechanism in which local shards were dissolved, with or without the presence of a gel phase, and reprecipitated within the same local volume. This process could have occurred on a shard-sized scale because the dissolution of a rhyolite glass shard will yield a composition similar to silica and any of the zeolites represented.

Iijima (1971) noted that clinoptilolite analyses determined by electron microprobe were anomalously high in silica and attributed this to finely divided silica mixed with the zeolite. Several similar observations were found in the course of the present work as well.

Na was either leached from the beds or exchanged with K prior to zeolitization. Perlite textures point to the likelihood of Na leaching, since Na loss usually accompanies the early stages of glass hydration (Jezek and Noble, 1978). A transfer of Na could have had an important influence on the resultant assemblage because ferrierite, although almost invariably containing minor Na, does not prefer it as mordenite does. Furthermore, although reactions in the presence of high  $a_{Na}$  could have precipitated phases such as albite or analcime, such relations are not found at Lovelock. Presumably because the prevailing silica concentrations were high, mordenite is the main Na-bearing phase. It is possible that low Na concentrations were necessary in addition to high Mg concentration in order that large quantities of ferrierite could crystallize.

The onset of ferrierite crystallization did not require the complete dissolution of the shards because it initially formed within primary pores and utilized glass and clays as substrates. The coarse tuff sample 4-8.5 is an example in which a mostly vitric tuff shows incipient ferrierite crystallization (Fig. 7). Here, where pore space was ample, the prismatic habit developed. The ferrierite-rich tuff SR67 provides an example of a case where the space was more limited or in which the activity of K was sufficiently high. As a consequence, finer, more massive ferrierite co-crystallized with orthoclase (Fig. 8). In this case, the habit of ferrierite is not obvious. Figure 8 illustrates the chemical heterogeneity within microscopic zones in many of the tuffs. The clinoptilolite and cristobalite replaced the glass while the K-rich phases ferrierite and orthoclase together fill the primary pore space.

Ferrierite is a rarely occurring zeolite and is unusual for its Mg-rich composition. Studies of the known natural ferrierite compositions (Wise and Tschernich, 1976; Sameshima, 1986) reveal that, without exception, ferrierite is a high-silica zeolite with a narrow range of framework Si/Al ratios ( $\sim 4.5-6$ ) and that Mg is an essential ingredient. The conditions for ferrierite crystallization in the Lovelock deposit appear to require both high concentrations of silica, supplied by the rhyolite, and of Mg. Hawkins and Roy (1963) pointed out that clay minerals will normally crystallize from Mg-bearing solutions formed by glass dissolution. The fact that ferrierite is so abundant in the Lovelock deposit must depend not only on such influences as pH, temperature, and composition but also on the nature of structural units present in the fluids. Certainly the combination of high Mg and high Si was important for ferrierite to crystallize. It is also possible that a templating process analogous to that proposed for large organic cations in some synthetic zeolites (Barrer, 1981) was operative during diagenesis in the Lovelock deposit. As noted above, Mg has a special role in the ferrierite structure. The presence of hydrated Mg ions,

$\text{Mg}(\text{H}_2\text{O})_6^{2+}$ , in crystallizing fluids likely fostered the knitting together of the ferrierite tetrahedral framework. Because the K ions can reside indiscriminately in the ferrierite channels, responding to framework charge but not affected by stringent steric considerations, the K concentrations are probably an accident of the prevailing solution chemistry.

The differences in ferrierite composition from one bed to another are indicative of the local chemical control on ferrierite formation and the lack of homogenization of diagenetic fluids on a large scale. Which of the zeolites crystallized was a function of the chemical composition of the mineralizing fluid, and this, in turn, was controlled by the compositions of parent glass and the mineral fragments in the pyroclastic deposit. The ferrierite chemical data obtained by TEM/EDX also suggest (e.g., Fig. 15) that the aqueous chemistry can vary on a very fine scale, perhaps approaching the volume of a few pores. We know that pH can have a large effect on the proportions of Al and Si species in aqueous systems. For example, the ratio of two critical ionic species,  $\text{Si}(\text{OH})_4/\text{Al}(\text{OH})_4^-$ , may vary by as much as a factor of 4 between pH 9 and 10 (Mariner and Surdam, 1970). This diagenetic system is clearly one of several scales of mass transfer through time. The first event, magnesium smectite formation, was the result of widespread but heterogeneous influx of fluids into the tuffs. Crystallization of zeolites was apparently controlled on a much smaller scale.

#### ACKNOWLEDGMENTS

This work represents a portion of the first author's Ph.D. dissertation at Lehigh University. He wishes to thank Exxon Research and Engineering Co. for supporting this research and allowing its publication, and M.M.J. Treacy and A.J. Jacobson, in particular, for their encouragement. He is also grateful to Charles B. Sclar for his helpfulness as the major advisor. SIMS microscopy was provided by D.P. Leta and W.B. Lamberti of Exxon Research and Engineering Co. and is greatly appreciated. Reviews by R.J. Lander and an anonymous reviewer and editorial comments by D.L. Bish contributed to significant improvements in the manuscript.

#### REFERENCES CITED

- Barrer, R.M. (1981) Zeolites and their synthesis. *Zeolites*, 1, 130–140.
- Boles, J.R. (1972) Composition, optical properties, cell dimensions, and thermal stability of some heulandite group zeolites. *American Mineralogist*, 56, 1463–1493.
- Boles, J.R., and Coombs, D.S. (1975) Mineral reactions in zeolitic Triassic tuff, Hokonui Hills, New Zealand. *Geological Society of America Bulletin*, 86, 163–173.
- Boles, J.R., and Surdam, R.C. (1979) Diagenesis of volcanogenic sediments in a Tertiary saline lake; Wagon Bed formation, Wyoming. *American Journal of Science*, 279, 832–853.
- Brey, G., and Schmincke, H.-U. (1980) Origin and diagenesis of the Roque Nublo breccia, Gran Canaria (Canary Islands)—petrology of Roque Nublo volcanics, II. *Bulletin of Volcanology*, 43, 15–33.
- Broxton, D.E., Bish, D.L., and Warren, R.G. (1987) Distribution and chemistry of diagenetic minerals at Yucca Mountain, Nye County, Nevada. *Clays and Clay Minerals*, 35, 89–110.
- Cormier, W.E., and Sand, L.B. (1976) Synthesis and metastable phase transformations of Na-, Na,K-, and K-ferrierites. *American Mineralogist*, 61, 1259–1266.
- Davies, D.K., Almon, W.R., Bonis, S.B., and Hunter, B.E. (1979) Deposition and diagenesis of Tertiary-Holocene volcanics, Guatemala. *Society of Economic Paleontologists and Mineralogists Special Publication*, 26, 281–306.
- Goldstein, J.I., Costley, J.L., Lorimer, G.W., and Reed, S.J.B. (1977) Quantitative X-ray analysis in the electron microscope. *Scanning Electron Microscopy/1977*, 1, 315–323.
- Gottardi, G., and Galli, E. (1985) Natural zeolites. *Minerals and Rocks* 18, 409 p. Springer-Verlag, Berlin.
- Graham, R.P.D. (1918) On ferrierite, a new zeolitic mineral from British Columbia; with notes on some other Canadian minerals. *Transactions of the Royal Society of Canada*, 3 (12), 185–201.
- Hawkins, D.B., and Roy, R. (1963) Distribution of trace elements between clays and zeolites formed by hydrothermal alteration of synthetic basalts. *Geochimica et Cosmochimica Acta*, 27, 785–795.
- Hay, R.L. (1963) Stratigraphy and zeolitic diagenesis of the John Day Formation of Oregon. *University of California Publications in Geological Sciences*, 42, 199–262.
- (1966) Zeolites and zeolitic reactions in sedimentary rocks. *Geological Society of America Special Paper*, 85, 130 p.
- Heiken, G., and Wohletz, K. (1985) Volcanic ash, 246 p. University of California Press, Berkeley, California.
- Hildreth, W. (1979) The Bishop tuff: Evidence for the origin of compositional zonation in magma chambers. *Geological Society of America Special Paper*, 180, 43–75.
- Iijima, A. (1971) Composition and origin of clinoptilolite in the Nakanosawa tuff of Rumoi, Hokkaido. In *Molecular Sieve Zeolites—I, Advances in Chemistry Series*, 101, 334–341.
- Jezeq, P.A., and Noble, D.C. (1978) Natural hydration and ion exchange of obsidian: An electron microprobe study. *American Mineralogist*, 63, 266–273.
- Jones, J.B., and Segnit, E.R. (1971) The nature of opal I. Nomenclature and constituent phases. *Journal of the Geological Society of Australia*, 18 (1), 57–68.
- Keller, W.D., Hanson, R.F., Huang, W.H., and Cervantes, A. (1971) Sequential active alteration of rhyolitic volcanic rock to endellite and a precursor phase of it at a spring in Michoacan, Mexico. *Clays and Clay Minerals*, 19, 121–127.
- Leta, D.P. (1985) A high-resolution, single ion sensitivity video system for secondary ion microscopy. In A. Benninghoven, R.J. Colton, D.S. Simons, and H.W. Werner, Eds., *Secondary ion mass spectrometry (SIMS V)*, Springer Series in Chemical Physics, vol. 44, p. 232–234. Springer-Verlag, New York.
- Mahood, G. (1986) Waxing and waning magma chambers: A comparison of zoning in ignimbrites and plutons. *Fourteenth International Mineralogical Association Abstracts with Program*, 163.
- Mariner, R.H., and Surdam, R.C. (1970) Alkalinity and formation of zeolites in saline alkaline lakes. *Science*, 170, 977–980.
- Mason, B., and Sand, L.B. (1960) Clinoptilolite from Patagonia. The relationship between clinoptilolite and heulandite. *American Mineralogist*, 45, 341–350.
- Mumpton, F.A. (1960) Clinoptilolite redefined. *American Mineralogist*, 45, 351–369.
- Noh, J.H., and Kim, S.J. (1986) Zeolites from Tertiary tuffaceous rocks in Yeongil area, Korea. In Y. Murakami, A. Iijima, and J.W. Ward, Eds., *New developments in zeolite science and technology*, 28, p. 59–66. *Proceedings of the Seventh International Zeolite Conference*, Kodansha and Elsevier, Tokyo.
- Regis, A.J. (1970) Occurrences of ferrierite in altered pyroclastics in central Nevada. *Geological Society of America Abstracts with Program*, 2, 661.
- Sameshima, T. (1986) Ferrierite from Tapu, Coromandel Peninsula, New Zealand, and a crystal chemical study of known occurrences. *Mineralogical Magazine*, 50, 63–68.
- Sand, L.B., and Regis, A.J. (1968) Ferrierite, Pershing County, Nevada. In *Abstracts for 1966*, *Geological Society of America Special Paper*, 101, 189.
- Sheppard, R.A., and Gude, A.J., III (1968) Distribution and genesis of authigenic silicate minerals in tuffs of Pleistocene Lake Tecopa, Inyo County, California. *U.S. Geological Survey Professional Paper*, 597, 38 p.
- (1973) Zeolites and associated authigenic silicate minerals in tuff-

- aceous rocks of the Big Sandy formation, Mohave County, Arizona. U.S. Geological Survey Professional Paper, 830, 36 p.
- Sheppard, R.A., Gude, A.J., III, and Mumpton, F.A. (1983) Field trip stop 6, Lovelock zeolite deposit, Lovelock, Nevada. In F.A. Mumpton, Ed., International Committee on Natural Zeolites Zeo-Trip '83, p. 48–55. Allen Press, Lawrence, Kansas.
- Stanley, K.O., and Benson, L.V. (1979) Early diagenesis of high plains Tertiary vitric and arkosic sandstone, Wyoming and Nebraska. Society of Economic Paleontologists and Mineralogists Special Publication, 26, 401–423.
- Stewart, J.H., and Carlson, J.E. (1978) Geologic map of Nevada. U.S. Geological Survey, scale 1:500000.
- Vaughan, P.A. (1966) The crystal structure of the zeolite ferrierite. *Acta Crystallographica*, 21, 983–990.
- Wise, W.S., and Tschernich, R.W. (1976) Chemical composition of ferrierite. *American Mineralogist*, 61, 60–66.

MANUSCRIPT RECEIVED FEBRUARY 22, 1991

MANUSCRIPT ACCEPTED NOVEMBER 1, 1991